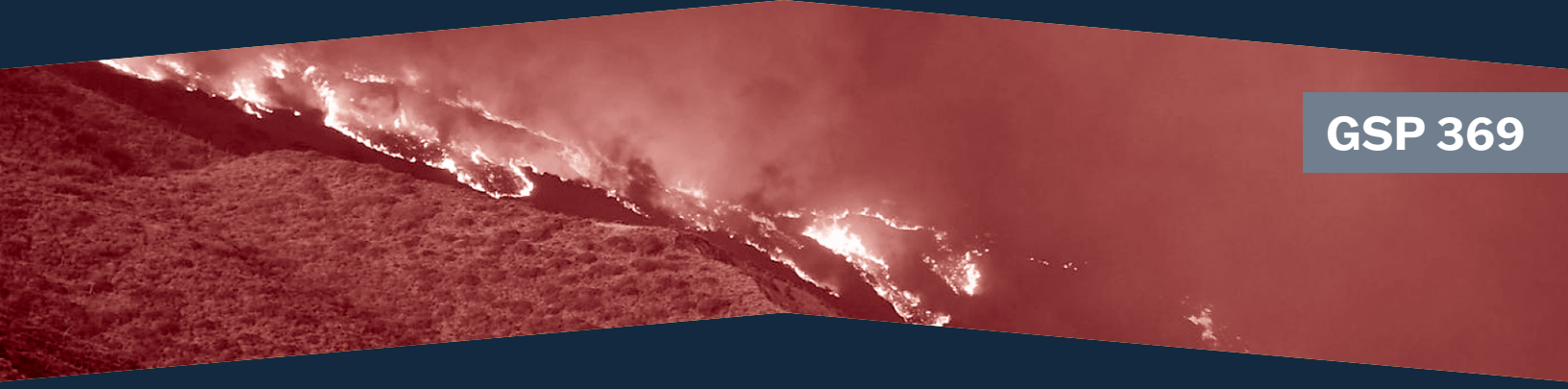


GSP 369

Geo-Extreme 2025



Remote Sensing, Instrumentation, Big Data, and Decision Making



Selected Papers from Geo-Extreme 2025
Long Beach, California • November 2–5, 2025

EDITED BY

Christopher L. Meehan, Ph.D., P.E., BC.GE;
James A. McKelvey III, Ph.D., P.E., BC.GE;
Adda Athanasopoulos-Zekkos, Ph.D.;
Miguel A. Pando, Ph.D., P.Eng.; Nina Stark, Ph.D.;
and Ming Xiao, Ph.D., P.E., BC.GE

ASCE

G-I ASCE GEO-INSTITUTE

GEOTECHNICAL SPECIAL PUBLICATION NO. 369

GEO-EXTREME 2025

REMOTE SENSING, INSTRUMENTATION, BIG DATA, AND DECISION MAKING

SELECTED PAPERS FROM GEO-EXTREME 2025

November 2–5, 2025
Long Beach, California

SPONSORED BY

The Geo-Institute
of the American Society of Civil Engineers

EDITED BY
Christopher L. Meehan, Ph.D., P.E., BC.GE
James A. McKelvey III, Ph.D., P.E., BC.GE
Adda Athanasopoulos-Zekkos, Ph.D.
Miguel A. Pando, Ph.D., P.Eng.
Nina Stark, Ph.D.
Ming Xiao, Ph.D., P.E., BC.GE

Published by the American Society of Civil Engineers

Published by American Society of Civil Engineers
1801 Alexander Bell Drive
Reston, Virginia, 20191-4382
www.asce.org/publications | ascelibrary.org

Any statements expressed in these materials are those of the individual authors and do not necessarily represent the views of ASCE, which takes no responsibility for any statement made herein. No reference made in this publication to any specific method, product, process, or service constitutes or implies an endorsement, recommendation, or warranty thereof by ASCE. The materials are for general information only and do not represent a standard of ASCE, nor are they intended as a reference in purchase specifications, contracts, regulations, statutes, or any other legal document. ASCE makes no representation or warranty of any kind, whether express or implied, concerning the accuracy, completeness, suitability, or utility of any information, apparatus, product, or process discussed in this publication, and assumes no liability therefor. The information contained in these materials should not be used without first securing competent advice with respect to its suitability for any general or specific application. Anyone utilizing such information assumes all liability arising from such use, including but not limited to infringement of any patent or patents.

ASCE and American Society of Civil Engineers—Registered in U.S. Patent and Trademark Office.

Photocopies and permissions. Permission to photocopy or reproduce material from ASCE publications can be requested by sending an e-mail to permissions@asce.org or by locating a title in ASCE's Civil Engineering Database (http://cedb.asce.org) or ASCE Library (http://ascelibrary.org) and using the "Permissions" link.

Errata: **Errata, if any, can be found at https://doi.org/10.1061/9780784486498**

Copyright © 2025 by the American Society of Civil Engineers.
All Rights Reserved.
ISBN 978-0-7844-8649-8 (PDF)
Manufactured in the United States of America.

Preface

The Embankments, Dams, and Slopes (EDS) Technical Committee of the ASCE Geo-Institute organized a timely and interesting specialty conference in 2021 in Savannah, Georgia, entitled *Geo-Extreme 2021: Geotechnical Engineering for Extreme Events*. This 2021 conference was intended as an inaugural specialty conference, and the beginning of a series of planned conferences organized by the EDS committee seeking to address the many societal challenges that are posed by extreme events such as: earthquakes, hurricanes, landslides, debris flows, wildfires, tornadoes, extreme rainfall events, blizzards, and other extreme loading events caused by changing weather patterns. This 2021 conference built on three previous slope stability related conferences that were organized by the EDS committee, two in 1966 and 1992 at the University of California at Berkeley and one in 2013 in San Diego. Strong impetus for that meeting was provided by a number of very significant extreme events in the United States, starting with Hurricanes Katrina in 2005 and Sandy in 2012 followed by Hurricanes Harvey, Irma, and Maria in 2017, and then Hurricanes Laura, Delta, and Zeta in 2020, which all caused widespread damage to communities at large, and particular damage to natural slopes and engineered structures that are the purview of the EDS Committee.

Since the 2021 conference, the onslaught of extreme loading events in the United States has continued unabated, with significant loss of life and severe financial consequences to communities that are unprecedented. The impact of major hurricanes including Ian, Ida, Idalia, Helene, and Milton has been strongly felt in coastal communities but also ranging far inland. Extreme rainfall and flood events have caused damages averaging in excess of a billion dollars annually, particularly in California. Severe storms, winds, and flooding also battered Kentucky heavily in 2025. Wildfires brought significant destruction and caused numerous deaths in Hawaii's Lahaina fire of 2023, the Smokehouse Creek fire in Texas and Oklahoma in 2024, and in California with the Park Fire in 2024 and wildfires in Southern California in 2025. The 2023 fire season was also particularly significant in Canada, which saw 45,700,000 acres of land burn across ten provinces and three territories.

Following these extreme events, the EDS Committee has proposed and organized the current specialty conference, *Geo-Extreme 2025: Geotechnical Engineering for Extreme Events*. The goal of this conference is to continue to draw attention to the pressing problems posed by extreme events, and to identify the critical role that geotechnical engineers and the civil engineering profession as a whole can play in mitigating the effects of these events, both before they occur, as well as after – that is, "building back safer" in a way that benefits both the built and natural environments.

Historical records show that the number of billion-dollar extreme events are on the rise. Mitigating the consequences of future extreme events requires geo-professionals taking timely actions, including evaluation of existing earthen structures, design and construction of protective structures in areas where an increased probability of damage is expected, refinement of existing geotechnical designs, and development of new adaptive measures and risk assessment tools. To achieve these objectives, the Geo-Extreme 2025 conference will comprise a multi-disciplinary forum between geotechnical engineers and other professionals from related disciplines, such as scientists, various

© ASCE

types of engineers, emergency managers, resilience and sustainability investigators, insurance experts, and policy makers, to provide solutions that properly cope with and address the wide variety of extreme events that can occur.

There are five volumes containing the full collection of papers presented at Geo-Extreme 2025: Geotechnical Engineering for Extreme Events, which was held on November 2-5, 2025, in Long Beach, California. These five volumes are subtitled: (1) Remote Sensing, Instrumentation, Big Data, and Decision Making, (2) Geotechnical Earthquake Engineering, (3) Civil Infrastructure, Geomaterials, and Case Histories, (4) Different Climates and the Coastal Zone, and (5) Permafrost, Wildfires, and Other Emerging Challenges in Geotechnical Engineering, respectively. These five volumes include over 130 contributions that span 25 subtopic areas of the conference, as noted in the subsequent tables of contents for each volume. Each of the five volumes are Geotechnical Special Publications (GSPs), containing papers that were reviewed in accordance with ASCE GSP standards. Each paper was subjected to technical review by two or more independent peer reviewers, and publication required concurrence by at least two peer reviewers.

The Editors gratefully acknowledge the immeasurable contributions of the countless individuals who made Geo-Extreme 2025 and these published proceedings possible, especially the reviewers, session chairs, organizing committee members, and ASCE staff listed in the acknowledgements.

The Proceedings Editors,

Christopher L. Meehan, Ph.D., P.E., BC.GE, F.ASCE, University of Delaware
James A. McKelvey, III, Ph.D., P.E., BC.GE, F.ASCE, Earth Engineering Incorporated
Adda Athanasopoulos-Zekkos, Ph.D., M.ASCE, University of California, Berkeley
Miguel A. Pando, Ph.D., P.Eng., M.ASCE, Drexel University
Nina Stark, Ph.D., M.ASCE, University of Florida
Ming Xiao, Ph.D., P.E., BC.GE, F.ASCE, Pennsylvania State University

© ASCE

Acknowledgments

The conference and its published proceedings would not have been possible without the diligent, coordinated effort of numerous people, especially the reviewers who provided detailed feedback on papers and the session chairs who made decisions and provided editorial assistance on selected topics. The editorial team is also profoundly grateful to Dr. Daniel Pradel and Dr. Navid Jafari (Conference Co-Chairs), the Technical Program Committee (listed below), Mr. Brad Keelor, Ms. Aurora Phlegar, and the ASCE publications team for their crucial roles in the production of these proceedings.

Geo-Extreme 2025 Conference Program Committee

Conference Co-Chairs

- Daniel Pradel, Ph.D., P.E., M.ASCE, *Ohio State University*
- Navid H. Jafari, Ph.D., M.ASCE, *Texas A&M University*

Technical Program Committee

- Timothy D. Stark, Ph.D., P.E., BC.GE, F.ASCE, *University of Illinois at Urbana-Champaign*
- James A. McKelvey, III, Ph.D., P.E., BC.GE, F.ASCE, *Earth Engineering Incorporated*
- Jeremy Varner, P.E., M.ASCE, *Federal Energy Regulatory Commission*
- Nazli Yesiler, Ph.D., A.M.ASCE, *California Polytechnic State University, San Luis Obispo*
- Ghada Ellithy, Ph.D., P.E., M.ASCE, *Embry-Riddle Aeronautical University*
- Stefan G. Flynn, P.E., M.ASCE, *US Army Corps of Engineers, Rock Island District*

Proceedings Editors

- Christopher L. Meehan, Ph.D., P.E., BC.GE, F.ASCE, *University of Delaware*
- James A. McKelvey, III, Ph.D., P.E., BC.GE, F.ASCE, *Earth Engineering Incorporated*
- Adda Athanasopoulos-Zekkos, Ph.D., M.ASCE, *University of California, Berkeley*
- Miguel A. Pando, Ph.D., P.Eng., M.ASCE, *Drexel University*
- Nina Stark, Ph.D., M.ASCE, *University of Florida*
- Ming Xiao, Ph.D., P.E., BC.GE, F.ASCE, *Pennsylvania State University*

© ASCE

Contents

Instrumentation and Remote Sensing of Extreme Events

Influence of Pore Fluid Temperature on the Performance of Electrical Conductivity Sensors for Assessing Pore Fluid Salinity Levels 1
William J. Baker III, Siamak Yoosefi, Mohammadreza Jebeli, and Christopher L. Meehan

Assessing Vetiver Grass Impact on Erosion Control and Infiltration of Yazoo Clay under Simulated Extreme Rainfall Conditions 13
Rahul Biswas, Asef Israk Arnob, Richa Pokhrel, and Sadik Khan

Continuous Monitoring System for Resilient Railway Infrastructure 25
A. Q. M. Zohuruzzaman, Mahdi Zulfikar, Sadik Khan, Brett Cobb, Abby Cisko, Thomas J. (Jeremy) Beasley, Ted Sussmann, and Hugh Thompson

Effects of Frontal Overlap on Checkpoint Errors in UAV Surveying: Corner and Inside Checkpoint Locations 34
Mohammadamin Nozari, William J. Baker III, and Christopher L. Meehan

Accuracy Evaluation of UAV-Based Orthophoto Mapping in Small, Semi-Planar Areas with Varying Control Point Configurations 44
Mohammadamin Nozari, Siamak Yoosefi, Mohammadreza Jebeli, and Christopher L. Meehan

Leveraging High-Resolution Data to Assess Coastal Dune Dynamics for Climate-Resilient Management in Katwijk, Netherlands 54
Caroline Y. Apraku, Amber Spears, and Reginald Archer

Big Data and Data Analytics for Extreme Events

Integration of Physics-Informed Neural Networks and Transfer Learning for Rainfall-Induced Landslide Forecasting 65
Shian Cao and Weibing Gong

Automating Ground Motion Quality Assessment Using Residual Neural Networks 75
Ali Namin, Albert Kottke, and Mohsen Zaker Esteghamati

A Physics and Reliability-Informed Machine Learning Framework for Landslide Susceptibility Assessment: A Case Study in Niang-niang-pa, Gansu, China 86
Hong-Zhi Cui, Te Pei, Jia-Xu Jin, and Jian Ji

© ASCE

Physics-Informed Machine Learning Framework for Predicting Rainfall-Induced Shallow Landslides in the Colorado Front Range 97
Te Pei, Marjan Maroufi, Chaopeng Shen, and Yingli Tian

Towards Robust and Adaptive Bearing Capacity Prediction for Dry Shallow Foundations Using Physics-Informed Machine Learning 107
Ekansh Agarwal, Te Pei, and Ning Luo

Application of Explainable Theory-Guided Machine Learning-Based Modeling to Rocking Foundations during Earthquake Loading 118
Sivapalan Gajan and Christopher Kantor

Decision Making, Planning, and Risk Management of Extreme Events

Case Studies on Unified Responses to Extreme Events via Geological Hazard Abatement Districts (GHADs) 128
Jeffrey A. Adams, Uri Eliahu, Haley Ralston, and Josef J. Tootle

Enhancing Power Grid Resilience: The Role of Trenchless Methods in Undergrounding High-Voltage Lines.....137
Samuel E. Brancheau, John H. Diamond, and Dennis J. Doherty

Geohazards Related to Karst in the State of Qatar: Towards the Elaboration of Geohazards/Risks Maps and Guidelines 145
J. Perrin, R. Couëffé, G. Noury, A. Ortiz, C. Allanic, T. Vilmus, J. Daranlot, B. Lemaire, O. Higgins, B. Matti, C. Lerevenu, A. Schönrock, R. Al-Dous, R. Pillai, S. A. Al-Yafei, E. A. Ahmed, U. S. Samad, H. A. Samman, and N. T. Mahmood

Predictive Detection of Soil Cavities in Embankments due to Culvert Defects Using Centrifuge Modeling and Image Analysis 155
Joelle Westcott and April Bowman

Leveraging Geofencing and Online Ad Campaigns for Enhanced Risk Communication in Hazard-Prone Areas 164
Noah C. Maddox

Deriving Optimal Evacuation Pathways to Reduce Evacuation Time for Underground Geotechnical Structures during Extreme Disasters 173
Hyunseok Kim, Mintaek Yoo, Yuseong Lee, Seokjung Kim, and Jinsun Lee

A Data-Driven Approach to Predicting the Stability of Root-Reinforced Slopes under Extreme Rainfall Conditions.....182
Sukrityranjan Samanta, Alba Yerro, and Swostika Dhakal

© ASCE

Geospatial Mosaic-Based 3D Ground Model of SPT-Derived Subsurface Stiffness in Seoul, South Korea.....194
Taek-Kyu Chung, Han-Saem Kim, Chang-Guk Sun, and Choong-Ki Chung

Development of Tunnel-Specific Depth-Damage Functions for Road Tunnels in Baltimore, MD.....202
Michael V. Martello

Defining Extreme Events with Practicable Monitoring Thresholds.....211
Patrick Grover, Madeline Hille, Caroline Scheevel, and Vincenzo Coia

Reducing the Extreme in Extreme Events by Knowing What Is Possible.....220
Mark Vessely, Scott Anderson, Zac Sala, Madeline Hille, Alex Brown, and Robert Group

Exploring the Impact of Extreme Rainfall on Risk and Resilience of Transportation Corridors Paralleling Rivers in Steep Terrain 234
Derrick Dasenbrock

© ASCE

Influence of Pore Fluid Temperature on the Performance of Electrical Conductivity Sensors for Assessing Pore Fluid Salinity Levels

William J. Baker III, Ph.D., A.M.ASCE[1]; Siamak Yoosefi, S.M.ASCE[2]; Mohammadreza Jebeli, S.M.ASCE[3]; and Christopher L. Meehan, Ph.D., P.E., F.ASCE[4]

[1]NRC Research Associate, Turner-Fairbank Highway Research Center, Federal Highway Administration, McLean, VA. ORCID: https://orcid.org/0000-0002-2243-8826. Email: William.J.Baker.ctr@dot.gov
[2]Ph.D. Student, Dept. of Civil, Construction, and Environmental Engineering, Univ. of Delaware, Newark, DE. ORCID: https://orcid.org/0000-0001-7884-5503. Email: siamakys@udel.edu
[3]Ph.D. Student, Dept. of Civil, Construction, and Environmental Engineering, Univ. of Delaware, Newark, DE. ORCID: https://orcid.org/0009-0003-0698-1196. Email: jebeli@udel.edu
[4]Professor, Dept. of Civil, Construction, and Environmental Engineering, Univ. of Delaware, Newark, DE. ORCID: https://orcid.org/0000-0002-9721-6275. Email: cmeehan@udel.edu

ABSTRACT

Rising sea levels, coastal land subsidence, and saltwater inundation caused by extreme events such as hurricane storm surge or tsunamis can affect a variety of natural phenomena, including coastal ecosystems and freshwater resources. Accurate monitoring of pore fluid salinity over time is critical for understanding the implications of elevated salinity levels on these natural phenomena. Traditionally, salinity levels in pore fluids are inferred using electrical conductivity sensors. It has been well established that pore fluid temperature influences the associated electrical conductivity measurements, necessitating the need to normalize electrical conductivity measurements to a reference temperature, e.g., 20°C or 25°C. However, previous research conducted by the authors revealed that the normalized electrical conductivity measured by some commercially available electrical conductivity sensors is still influenced by pore fluid temperature, requiring the development of calibration models to improve sensor performance. This study expands on previous work conducted by the authors by performing an experimental study to assess the impact of pore fluid temperature on electrical conductivity measurements using five commercially available electrical conductivity sensors. Each of the five sensors was tested in a variety of saline solutions with nominal electrical conductivity levels ranging from 100 µs/cm to 100,000 µs/cm. Each saline solution was also subjected to thermal loading with temperatures ranging from 5°C to 50°C in 5°C increments, in order to assess the influence of pore fluid temperature on sensor performance. A calibration procedure previously developed by the authors was also implemented to evaluate its effectiveness with respect to improving sensor performance under a variety of thermal loading conditions. Findings from this study help provide interested readers a protocol for improving sensor performance to better assess the impacts of increasing salinity levels over time in coastal soils.

INTRODUCTION

Rising sea levels, coastal land subsidence, and saltwater inundation caused by extreme events such as hurricane storm surge or tsunamis can cause a variety of geotechnical engineering

© ASCE

problems, including increased erosion of coastal shorelines, increased flooding events that will impact roadways and foundation systems, and increased saltwater intrusion into coastal soils and freshwater aquifers (Burke-Flask et al., 2021). In particular, saltwater intrusion has the potential to alter the geotechnical properties of non-saline soils including their shear strength behavior (e.g., Tiwari and Ajmera, 2015; Jebeli et al., 2025b, Yoosefi et al. 2025), hydraulic conductivity behavior (e.g., Tang et al., 2021, Jebeli et al., 2025a), and compressibility behavior (e.g., Tiwari and Ajmera, 2014; Yoosefi et al., 2024a). The use of field sensors for monitoring and measuring changes in the amount of salt present (e.g., salinity) within the pore fluid of a soil is of critical importance in order to properly forecast potential changes in the mechanical behavior of soils and, consequently, the performance of civil infrastructure in coastal regions.

Historically, electrical conductivity sensors have been heavily utilized as a reliable means to infer the salinity level of the pore fluid within soils (Hendrickx et al., 2002). However, the electrical conductivity of a pore fluid is influenced by the temperature of the pore fluid (e.g., Slavich and Petterson, 1990), as higher pore fluid temperatures result in increased mobility of the ions present in the pore fluid resulting in an increase in the apparent electrical conductivity within the pore fluid. This phenomenon is well known, as other researchers have indicated that the electrical conductivity of a pore fluid increases at an approximate rate of 1.9% per °C (Corwin and Lesch, 2005). Consequently, electrical conductivity sensors have typically normalized electrical conductivity measurements at a reference temperature (e.g., 25°C, METER Group (2020 and 2021)). However, research previously conducted by the authors has shown that even these normalized electrical conductivity measurements are still affected by temperature fluctuations and may require calibration equations to remove these artifacts (e.g., Baker et al., 2025; Yoosefi et al., 2024b). Therefore, to assess the potential impacts of temperature on normalized electrical conductivity measurements, an experimental investigation was performed by subjecting five commercially available electrical conductivity sensors to various saline solutions with electrical conductivities ranging from 100 µS/cm to 100,000 µS/cm, which were in turn subjected to temperature changes over a range from 5°C to 50°C. It should be noted that the experimental investigation conducted within the current study is an expansion of the initial investigation conducted by Baker et al. (2025), who only considered three commercially available electrical conductivity subjected to thermal loading conditions ranging from 20°C to 50°C. The proceeding sections of this study provide details regarding the experimental procedure that was utilized, followed by the corresponding results and calibration procedure for correcting for potential deviations in electrical conductivity due to changes in pore fluid temperature.

EXPERIMENTAL PROCEDURE

Sensor Selection

Five commercially available electrical conductivity sensors were selected to investigate the potential influence of pore fluid temperature on the performance of these sensors (e.g., change in *normalized* electrical conductivity measurements due to changes in temperature). Two of the sensors (i.e., Sensor 1 –TEROS12 and Sensor 2 – TEROS15, both manufactured by METER Group) measure the electrical conductivity of the pore fluid by applying an alternating current between two electrodes that are housed within steel needles and measuring the resulting resistance. The other three conductivity sensors (i.e., Sensor 3 – Insitu Aqua TROLL 100, Sensor 4 – Soilnst Level Logger LTC5, and Sensor 5 – METER Group ES2) utilize a 4-Electrode

© ASCE

Platinum configuration to measure electrical conductivity. More specifically, one pair of electrodes (i.e., the outer poles) are used to measure the voltage drop between the pair by applying an alternating current, while the other pair of electrodes are used to measure the current flow between the pair. When using this specific configuration, the conductance (converted to electrical conductivity by multiplying by a cell constant) is determined by the ratio of current to voltage within the solution. It should also be mentioned that each of the five sensors used in the current study had a built-in thermistor to measure the pore fluid temperature. A summary of the electrical conductivity and temperature specifications for each of the five sensors are provided in Table 1. It should be noted that these five particular electrical conductivity sensors were chosen because they are all currently deployed by several research groups at the University of Delaware who are monitoring a number of fragile coastal sites (e.g., Joshi et al., 2023; Baker et al., 2024) to develop a more specific understanding of the effect of changes in salinity due to flooding, land subsidence, coastal storm effects, and sea level rise on the geotechnical, chemical, and biological properties of soils.

Table 1. Specifications of Electrical Conductivity Sensors

Sensor		Electrical Conductivity		Temperature Range	
I.D.	Make/Model	Range (μs/cm)	Accuracy	Min (°C)	Max (°C)
Sensor 1	METER Group TEROS12	0 - 20,000	±5% to ±8%†	-40	60
Sensor 2	METER Group TEROS15	0 - 20,000	±2%	-40	60
Sensor 3	Insitu Aqua TROLL 100	0 - 100,000	±0.5 to ±1%‡	-5	50
Sensor 4	Soilnst Level Logger LTC5	0 - 100,000	±1 to ±2%††	-20	80
Sensor 5	METER Group ES2	0 - 120,000	±10%	-40	60

† - ±5% for conductivity from 0 μS/cm – 10,000 μS/cm, ±8% for conductivity from 10,000 μS/cm – 20,000 μS/cm

‡ - ±0.5% for conductivity from 1 μS/cm – 80,000 μS/cm, ±1% for conductivity > 80,000 μS/cm

†† - ±1% for conductivity from 5,000 μS/cm – 80,000 μS/cm, ±2% for conductivity from 50 μS/cm – 5,000 μS/cm

The electrical conductivity measured by Sensor 1, Sensor 2, and Sensor 5 are normalized to an electrical conductivity at 25°C using Equation 1 as specified by the manufacturer (METER Group 2020, 2021):

$$EC_{25} = \frac{EC_T}{1+0.019(T-25)} \quad (1)$$

where EC_{25} is the bulk electrical conductivity measured by the sensor corresponding to a temperature of 25°C, and EC_T is the corresponding bulk electrical conductivity at temperature T, which is recorded by the sensor in °C. The electrical conductivity measured by Sensor 3 and Sensor 4 are not normalized to a standard temperature. Therefore, for comparison purposes within the framework of the current study, the electrical conductivities measured by Sensor 3 and Sensor 4 were normalized to an electrical conductivity at 25°C using Equation 1.

© ASCE

Experimental Set-Up and Procedure

Various aqueous saline solutions were prepared using anhydrous sodium chloride (NaCl, purity > 99.0%) as the solute. NaCl was chosen as the solute as opposed to potassium chloride (KCl, which is typically the recommended solute to perform independent calibrations of electrical conductivity, e.g., ISO 11265, 1994) as Baker et al. (2025) performed a similar experimental study as the one outlined in the current study utilizing KCl as the solute. Although standards such as ASTM D1125-23 and ISO 7888-85 specify the use of KCl for calibration purposes, NaCl was intentionally used in this study to allow for a broader validation of sensor performance across a range of ionic types (e.g., Na^+ versus K^+) to further enhance the robustness of the proposed calibration methodology originally proposed by Baker et al. (2025). Additionally, NaCl is the primary electrolyte found in saline solutions found in marine and estuarine environments (e.g., ASTM D1141-21). Saline solutions were prepared by mixing 20 kg of distilled, deionized water with predetermined amounts of NaCl in order to achieve a specific level of electrical conductivity (e.g., 1.168 g NaCl per kg of distilled water = 2,000 μs/cm). An analytical balance (with a precision of 0.0001 g) was utilized to measure the required amount of NaCl to achieve a specific electrical conductivity level for each solution as precisely as possible. Mixing each saline solution to a homogenous state was performed using a magnetic mixer with a mixing speed of 1600 rpm. It should be noted that the magnetic mixer could only mix 10 kg of solution at a time, requiring two batches to be mixed for a given experiment. Homogenous mixing of each saline solution was achieved after approximately ten minutes of mixing.

Upon completion of the mixing process, each saline solution was transferred to a tempered, hermetically sealed plastic container that had nominal dimensions of 58.4 cm long by 41.3 cm wide by 31.4 cm deep (e.g., 53 L in volume). All five of the electrical conductivity sensors were placed inside the plastic container by affixing each sensor to a steel rod and securing each rod using connectors and standard chemistry ring stands. Care was taken to ensure that Sensor 1 and Sensor 2 were placed far enough away from the other sensors, as these sensors have a volume of influence of approximately 1,010 mL (METER Group, 2020). A Resistance-Temperature Device (RTD) probe utilizing a 100Ω platinum resistor was also placed within the saline solution to monitor the temperature changes of the saline solution during testing and provided an independent check against each of the built-in thermistors for each of the conductivity sensors used in this study. In an aggregate sense, each of the sensors' built-in thermistors under-measured temperature by -0.6°C to -0.3°C relative to the temperature measured by the RTD probe for each of the experiments performed within this study.

During a given experiment, the temperature of the saline solution was regulated from 5°C to 50°C in 5°C increments. This temperature range was selected to expand upon the temperature regimes utilized by Baker et al. (2025) and Yoosefi et al. (2024b) when evaluating the temperature sensitivity of their sensors while also ensuring not to exceed the manufacturer's specified temperature range for each sensor (Table 1). Temperature regulation of the saline solution at a desired temperature for testing was achieved using both a ½ horsepower water chiller and two commercially available immersion circulators (e.g., "sous vide" immersion circulators that are commonly used to achieve a constant fluid temperature when cooking). The water chiller was used to cool the saline solution from its nominal room temperature (e.g., 18°C ±1°C) down to the initial desired temperature of 5°C. 'Thermal loading' of the saline solution from 5°C to 15°C in 5°C increments was achieved by setting the temperature of the water chiller to the desired testing temperature (e.g., 10°C or 15°C) while also setting the temperature of the

© ASCE

immersion circulators to 20°C. If the current temperature of the saline solution was less than the desired testing temperature, the water chiller would not chill the solution. Therefore, the immersion circulators were used to heat the solution to the desired testing temperature. Once the desired testing temperature within this thermal loading regime was reached, the immersion circulators were turned off and the water chiller was used to maintain the desired temperature. Thermal loading of the saline solution from 20°C to 50°C in 5°C increments was achieved utilizing the immersion circulators, while the water chiller was turned off during this stage of testing for a given experiment.

Figure 1 provides a nominal thermal loading regime for a given experiment conducted within this study. Once each conductivity sensor had reached the specific temperature based on their respective thermistor measurements, the temperature of the saline solution was held constant for approximately 15 minutes to ensure an adequate amount of data was collected for a given temperature. For data collection purposes, Sensor 1, Sensor 2, and Sensor 5 were wired into a CR6 data logger (Campbell Scientific 2022), which was connected to a laptop to allow for real-time data collection. Sensor 3 and Sensor 4 both have a built-in data logger and therefore were directly connected to the aforementioned laptop for real-time data collection. The sampling rate for all three sensors was set to a frequency of 0.5 Hz (e.g., 1 sample every 2 seconds). It should be emphasized that before each electrical conductivity measurement, each sensor was thoroughly washed with distilled, deionized water to remove any salt residue from the previous experiment. This procedure was repeated for eight different saline solutions prepared with target conductivities of 100, 500, 1,000, 2,000, 5,000, 10,000, 20,000, 50,000, and 100,000 µs/cm. The concentration of these saline solutions was determined by considering the salinity levels utilized by Baker et al. (2025) along with considering the maximum sensor conductivity ranges outlined in Table 1.

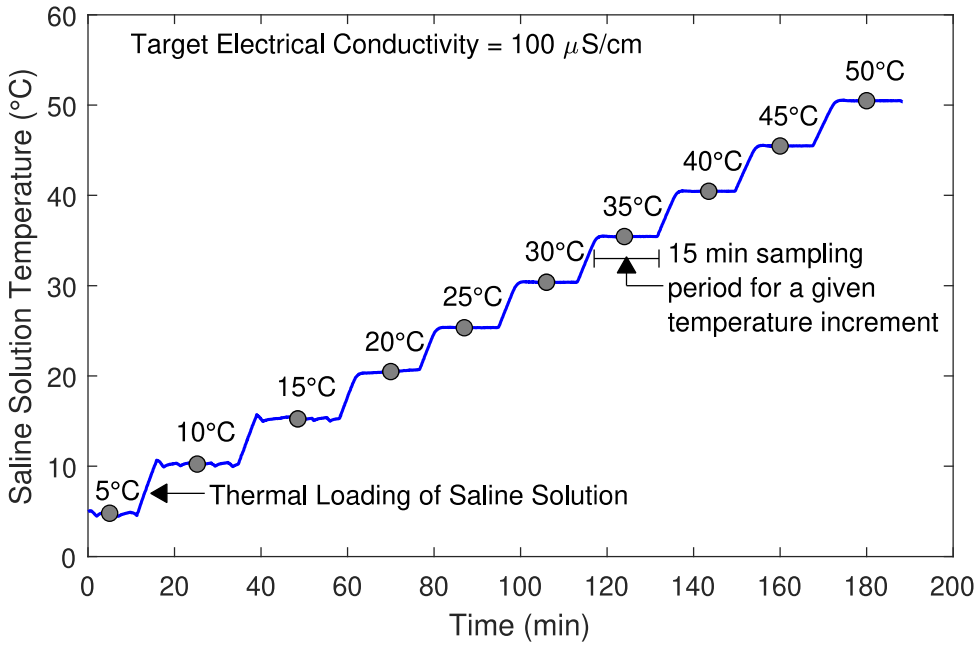


Figure 1. Nominal thermal loading procedure of saline solution.

© ASCE

RESULTS

Figure 2 provides nominal results from a given experiment (e.g., a target conductivity for the saline solution = 1,000 μs/cm) showing the influence of pore fluid temperature on the *normalized* electrical conductivity (i.e., E_{25} from Equation 1) measured from each of the five electrical conductivity sensors. Figure 2a shows all of the measurements that were collected during the experiment (e.g., at a sample rate of 0.5 Hz), while Figure 2b shows the average normalized electrical conductivity at each of the specified temperatures (for the 5°C to 50°C range in 5°C increments). Averaging was performed to help better visualize the potential influence of temperature on the normalized electrical conductivity measurements. Overall, the results shown in Figure 2 indicate that the temperature of the saline solution influenced the normalized electrical conductivity measurements of each of the five sensors. However, this influence varied between sensors. More specifically, Sensors 1, 2, and 5 showed positive trends (e.g., an increase in normalized electrical conductivity with an increase in temperature), Sensor 3 showed a negative trend (e.g., a decrease in normalized electrical conductivity with an increase in temperature), and Sensor 4 showed little to no trend with respect to increase in pore fluid temperature. These trends are best visualized in Figure 2b. Along with each sensor being influenced by pore fluid temperature by varying degrees, some sensors also exhibited more noise/scatter relative to other sensors. This is shown in Figure 2a, where the bandwidth of the normalized electrical conductivity readings measured by Sensor 1 is significantly greater relative to the other four sensors. More specifically, the coefficient of variation (COV) of the normalized electrical conductivity at a specific temperature interval for Sensor 1 was generally two to five times higher relative to the COV of the normalized electrical conductivity measured by the other four sensors used in this study.

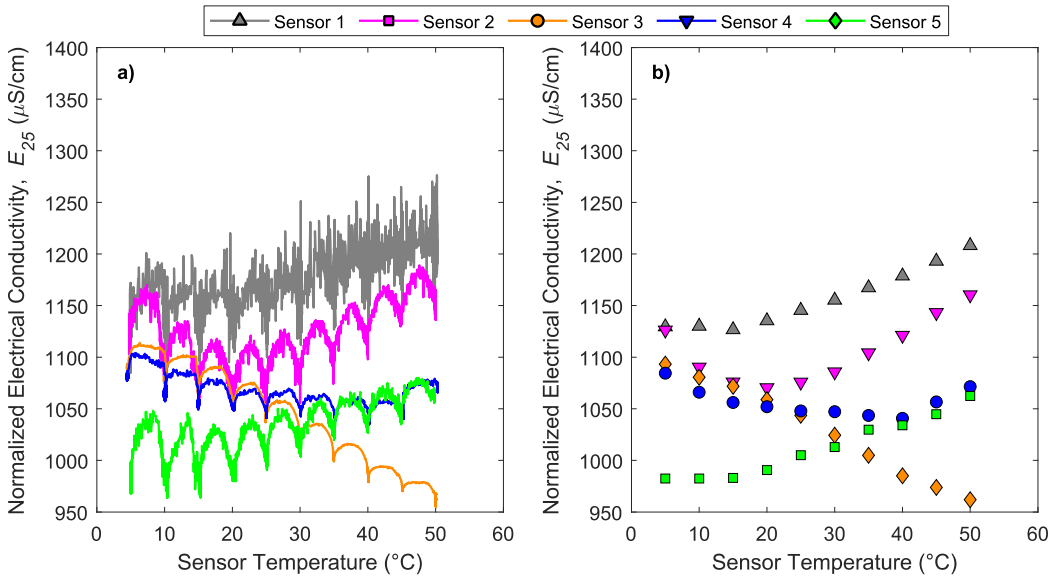


Figure 2. Influence of pore fluid temperature on normalized electrical conductivity: a) all measurements, and b) average measurements (nominal salinity of solution = 1,000 μs/cm).

Figure 3 shows the overall performance of each of the five sensors utilized. More specifically, Figure 3 shows boxplots (e.g., distribution of all normalized electrical conductivity

© ASCE

measurements) for each of the nine (9) saline concentrations tested within the current study. It should be noted that for Sensor 1 and Sensor 2, boxplots are only shown for target electrical conductivity values up to 20,000 µS/cm based of the sensor's specifications outlined in Table 1. For comparison purposes, normalized electrical conductivity measurements for a given target concentration were divided by the target concentration as indicated by the y-axes in Figure 3 (e.g., $E_{25,sensor}/ E_{25,target}$). Similarly, solid lines were drawn at $E_{25,sensor}/ E_{25,target}$ values of 1, while dashed lines were drawn at $E_{25,sensor}/ E_{25,target}$ values of 0.9 and 1.1 to indicate sensor accuracy based on the values outlined in Table 1 (e.g., ±10%). When interpreting the results shown in Figure 3, boxplots with longer lengths for a given target electrical conductivity concentration indicate that a particular sensor was more sensitive to temperature changes relative to another sensor. Accordingly, visual inspection of Figure 3 reveals that in a general sense, Sensors 4 and 5 were the least sensitive to temperature changes given the relative length of each boxplot for these sensors (with the exception of the boxplot for Sensor 4 corresponding to a target electrical conductivity of 100,000 µS/cm, which is the maximum electrical conductivity the sensor is rated for). Similarly, Sensor 3 showed the best performance out of the five sensors tested, as all nine of the sensor's boxplot distributions were generally within the ±10% band.

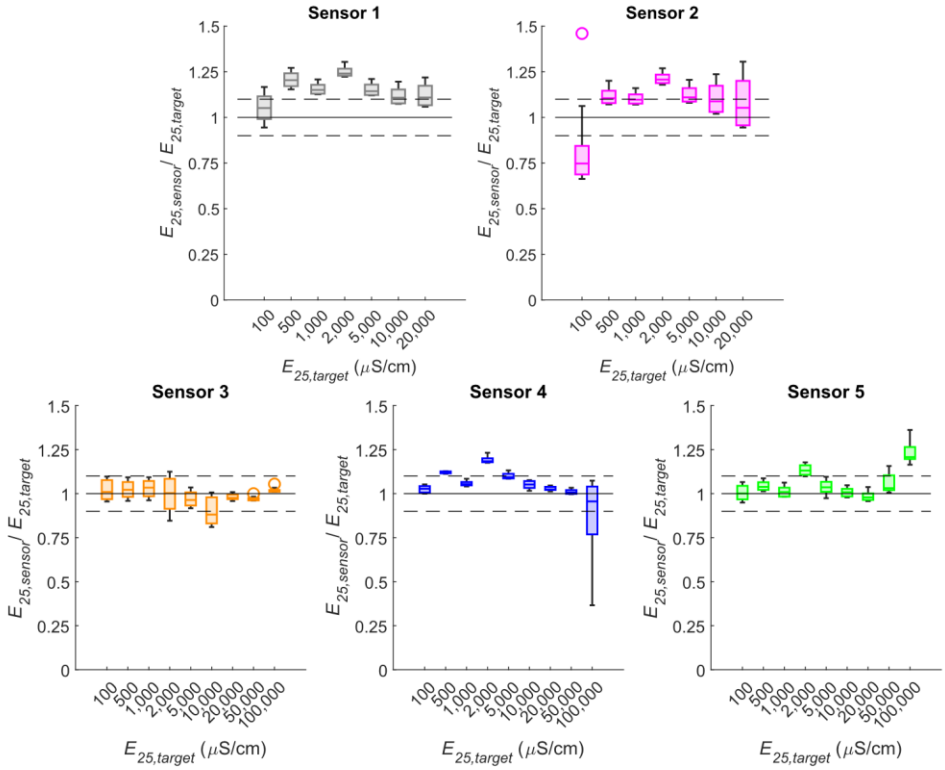


Figure 3. Overall performance for each of the five sensors tested within the current study.

CALIBRATION PROCEDURE

The temperature sensitivity of a particular sensor can be quantified by performing linear regression analysis at a given electrical conductivity concentration (e.g., performing linear regression analysis on the results shown in Figure 2b) using the following functional form (e.g., Meehan and Talebi, 2017):

© ASCE

$$EC_{25}(T) = m_T T + EC_{25,0} \quad (2)$$

where $EC_{25}(T)$ is the normalized electrical conductivity measured by each sensor, m_T is the slope calculated from the linear regression analysis, T is the temperature of the saline solution recorded by a given sensor in ℃ and $EC_{25,0}$ is the apparent electrical conductivity measurement that would be measured at a solution temperature of 25℃. To correct for potential temperature dependence of the E_{25} measured for a given sensor, the following equation can be implemented:

$$EC_{25,cor}(T) = EC_{25}(T) - m_T(T - T_{in}) \quad (3)$$

where $EC_{25,cor}(T)$ is the normalized electrical conductivity corrected for variations in temperature, m_T is the slope calculated from the linear regression analysis using Equation 2, T is the temperature of the saline solution recorded by the sensor in ℃ and T_{in} is the initial temperature of the saline solution recorded by the sensor. Initially, Baker et al. (2025) showed that for some types of electrical conductivity sensors, the variation of m_T as a function of the electrical conductivity concentration can be quantified using a power function. However, this power function may not be a suitable functional form for all conductivity sensors. A more generalized functional form for quantifying the variation of m_T as a function of electrical conductivity concentration is a two-term polynomial function as shown below:

$$EC_{25,cor}(T) = EC_{25}(T) - [(k_1 EC_{25}^2) + (k_2 EC_{25}) + k_3](T - T_{in}) \quad (4)$$

where k_1 through k_3 are regression coefficients. The resulting calibration procedure using this two-term polynomial function is shown in Figures 4 and 5 below for all five sensors tested within the current study.

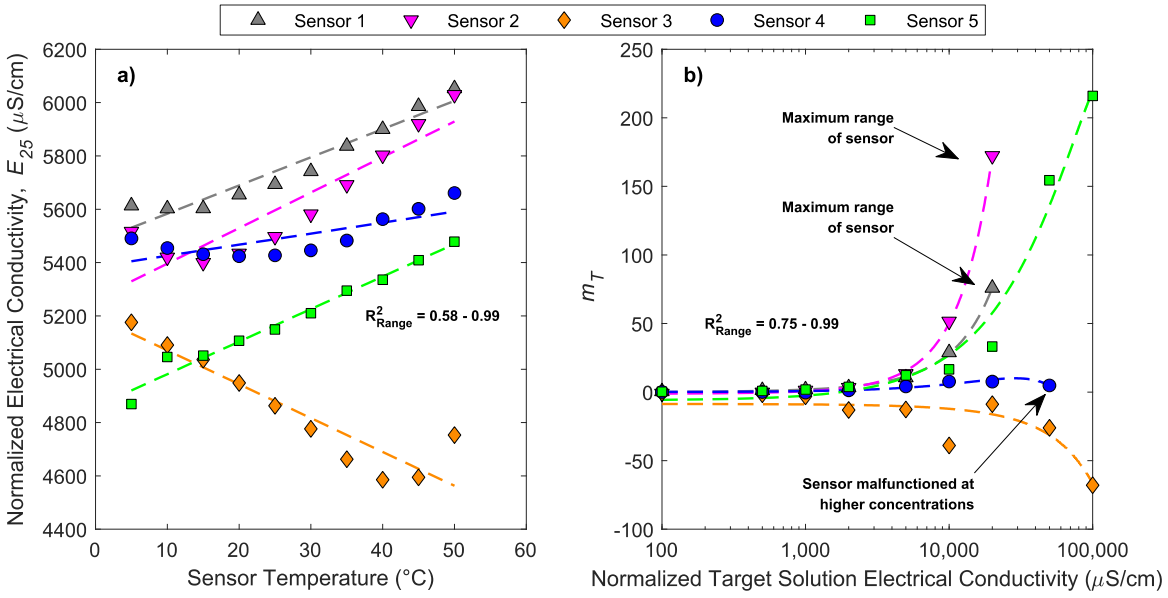


Figure 4. Proposed calibration procedure: a) determining m_T for a specific electrical conductivity concentration, and b) variation of m_T as a function of electrical conductivity concentration.

© ASCE

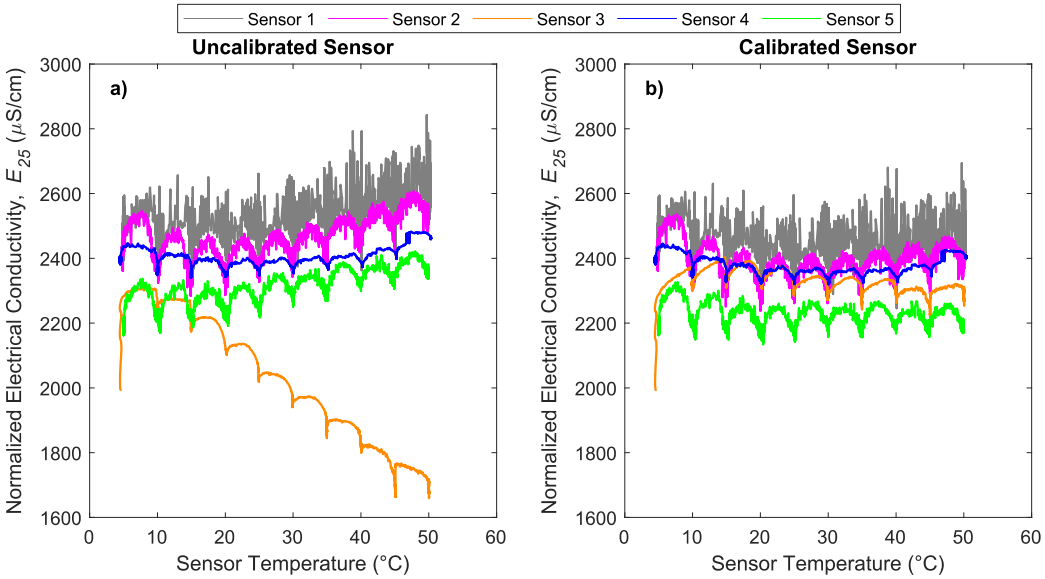


Figure 5. Results of calibration procedure to remove temperature dependence from E_{25} measurements: a) uncalibrated results, and b) calibrated results (nominal salinity of solution = 2,000 μs/cm).

It can be observed from the results shown in Figure 5 that the proposed calibration procedure can effectively remove the temperature dependence on the resulting E25 measurements for each sensor. However, the proposed calibration procedure does not take into account the observed cyclic fluctuations in E_{25} measurements with increasing temperature. This phenomenon is shown in Figure 6, which shows the electrical conductivity measurements measured by Sensor 2 after calibration for a nominal solution salinity of 2,000 μs/cm. Results shown in Figure 6 are presented as a scatter plot to help visualize this observed cyclic behavior post-calibration. As shown, as the temperature increases from one temperature increment to another, a bell-shaped curve is observed, which is consistent for each of the temperature increments across the entire temperature regime. However, once the temperature is stabilized at a given temperature, the corresponding electrical conductivity measurements also stabilize, which holds true for each of the temperature increments across the entire temperature regime. This fluctuation in electrical conductivity measurements due to rapid changes in temperature is most likely attributed to the *thermal lag effect* (Garau et al., 2011). More specifically, the thermal lag effect is a phenomenon where the temperature of the conductivity cell housed inside the sensor lags behind the temperature of the solution it is measuring when exposed to a temperature gradient. Consequently, this lag in temperature can potentially result in erroneous conductivity measurements, especially when solutions are exposed to strong temperature gradients (Garau et al., 2011). However, this observed phenomenon is most likely attributed to the strong temperature gradient each of the sensors was exposed to during a given experiment (e.g., 15°C/hr, calculated from Figure 1), which is sixty (60) times greater than the maximum temperature gradient observed when these sensors are deployed in a field environment (e.g., 0.25°C/hr, Baker et al., 2024). Therefore, this thermal lag effect should not reduce the effectiveness of the proposed calibration procedure when this calibration approach is applied to electrical conductivity sensors that are being deployed in a field environment.

© ASCE

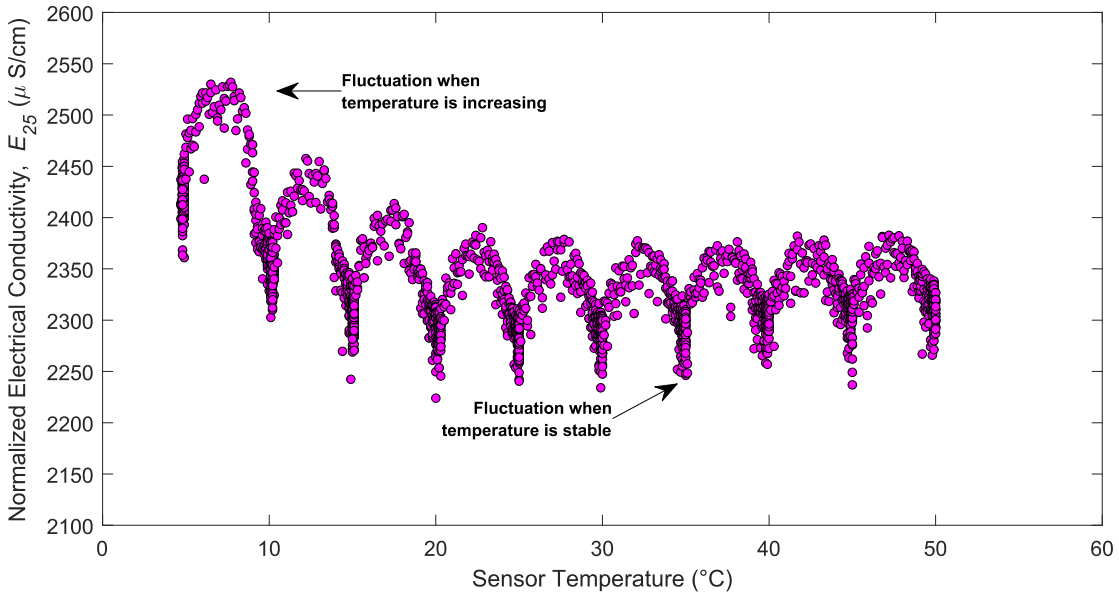


Figure 6. Fluctuations in normalized electrical conductivity measurements of Sensor 2 after calibration (nominal salinity of solution = 2,000 μs/cm).

CONCLUSIONS

The ability to accurately measure electrical conductivity within a soil's pore fluid is extremely important for monitoring changes in salinity in the pore fluid over time. This study examined the temperature sensitivity of five commercially available electrical conductivity sensors in saline solutions (e.g., NaCl solutions) with nominal electrical conductivity levels ranging from 100 μs/cm to 100,000 μs/cm. Each saline solution was subjected to thermal loading with temperatures ranging from 5°C to 50°C, with measurements recorded in 5°C increments. Results from this study indicated that all five of the sensors' *normalized* electrical conductivity measurements (e.g., E_{25}) exhibited some level of sensitivity to temperature changes. A calibration framework was proposed that provided an effective approach to removing the temperature dependence on the resulting E_{25} measurements for three of the five sensors. Observed cyclic fluctuations in E_{25} measurements post-calibration are most likely attributed to the thermal lag phenomenon due to the high thermal gradient imposed during laboratory testing. However, the proposed calibration procedure remains effective for field deployments, where temperature gradients are significantly lower. Ultimately, the results from this study highlight the importance of performing independent calibrations of a given electrical conductivity sensor prior to deploying the sensor in the field.

ACKNOWLEDGEMENTS

This material is based upon work supported by the US Army Engineer Research and Development Center under Award ID: W912HZ-20-2-0041. This project was supported in part by an appointment to the NRC Research Associateship Program at the Federal Highway Administration, administered by the Fellowships Office of the National Academies of Sciences, Engineering, and Medicine. Partial support for this work was provided by the Federal Highway

© ASCE

Administration under contract number 693JJ323D000004. Any opinions, findings, conclusions, or recommendations expressed in this publication are those of the author(s) and do not necessarily reflect the views of the Federal Highway Administration.

REFERENCES

ASTM. ASTM D1125-23. (2023). *Standard Test Methods for Electrical Conductivity and Resistivity of Water*. Annual Book of ASTM Standards, Vol. 11.02, ASTM International, West Conshohocken, PA.

ASTM. ASTM D11141-98. (2021). *Standard Practice for Preparation of Substitute Ocean Water*. Annual Book of ASTM Standards, Vol. 11.02, ASTM International, West Conshohocken, PA.

Baker, W. J., Yoosefi, S., Jebeli, M., and Meehan, C. L. (2025). "Temperature Sensitivity of Three Conductivity Sensors for Measuring the Electrical Conductivity of Soil Pore Fluid." *Proc., GeoenvironMeet 2024: Climate Change and the Geoenvironment*, Louisville, KY, March 2-5, 2025, ASCE, Reston, VA. 98-107.

Baker, W. J., Yoosefi, S., Jebeli, M., and Meehan, C. L. (2024). "Instrumentation of a Natural Terrestrial Site to Assess Seasonal Variations in Temperature, Water Level, Pore Pressure, and Salinity." *Proc., Geo-Congress 2024:Geotechnical Site and Soil Characterization*, Vancouver, British Columbia, Canada, February 25–28, 2024, ASCE, Reston, VA. 187-197.

Burke-Flask, A., Stark, N., and Rodriguez-Marek, A. (2021). "Addressing Sea Level Rise from the Ground Up: Understanding the Implications for Coastal Geotechnics." *Proc., Geo-Extreme 2021: Case Histories and Best Practices*, Savannah, GA, November 7-10, 2021, ASCE, Reston, VA. 393-402.

Corwin, D. L., and Lesch, S. M. (2005). "Apparent Soil Electrical Conductivity Measurements in Agriculture." *Computers and Electronics in Agriculture*, 46(1), 11-43.

Garau, B., Ruiz, S., Zhang, W. G., Pascual, A., Heslop, E., Kerfoot, J., and Tintoré, J. (2011). "Thermal Lag Correction on Slocum CTD Glider Data." *Journal of Atmospheric and Oceanic Technology*, 28(9), 1065–1071.

Hendrickx, J. M. H., Das, B., Corwin, D. L., Wraith, J. M., and Kachanoski, R. G. (2002). "Indirect Measurement of Solute Concentration." In: Dane, J. H., Topp, G. C. (Eds.), *Methods of Soil Analysis, Part 4 – Physical Methods*. Soil Sci. Soc. Am. Book Ser. 5. Soil Science Society of America, Madison, WI, USA, pp. 1274-1306.

ISO. ISO 11265:1994. (1994). *Soil Quality – Determination of The Specific Electrical Conductivity*. Standard. International Organization for Standardization, Geneva, CH.

ISO. ISO 7888:1985. (1994). *Water Quality – Determination of Electrical Conductivity*. Standard. International Organization for Standardization, Geneva, CH.

Jebeli, M., Yoosefi, S., Baker, W. J., and Meehan, C. L. (2025a). "Experimental Study on the Effect of Salinity Variations on the Water Retention of a Marine Lean Clay and Kaolinite." *Proc., GeoenvironMeet 2025: Climate Change and the Geoenvironment*, Louisville, KY, March 2-5, 2025, ASCE, Reston, VA. 108-117.

Jebeli, M., Yoosefi, S., Baker, W. J., and Meehan, C. L. (2025b). "Effect of Pore Water Salinity on the Residual Strength of Kaolinite." *Proc., Geotechnical Frontiers 2025: Engineering Geology and Site Characterization*, Louisville KY, March 2-5, 2025, ASCE, Reston, VA. 456-464.

© ASCE

Joshi, S., Afsar, M., Yan, J., Gu, C., Jin, Y., and Sparks, D. L. (2023). "Salinity and Redox Oscillation Induced Changes in Phosphorus Bioavailability and Speciation in Tidal Salt Marsh Sediment." *The joint ICOBTE & ICHMET 2023*, Wuppertal, Germany, Sep. 6-10.

Meehan, C. L., and Talebi, M. (2017). "A Method for Correcting Field Strain Measurements to Account for Temperature Effects." *Geotextiles and Geomembranes*, 45(4), 250-260.

METER Group. (2020). "TEROS 11/12." Instruction Manual, METER Group, Court Pullman, WA.

METER Group. (2021). "ES-2." Instruction Manual, METER Group, Court Pullman, WA.

Slavich, P. G., and Petterson, G. H. (1990). "Estimating Average Rootzone Salinity from Electromagnetic Induction (EM-38) Measurements." *Australian Journal of Soil Research* 28(3) 453-463.

Tang, S., She, D., and Wang, H. (2021). "Effect of Salinity on Soil Structure and Soil Hydraulic Characteristics." *Canadian Journal of Soil Science*, 101(1), 62-73.

Tiwari, B., and Ajmera, B. (2014). "Effects of Saline Fluid on Compressibility of Clay Minerals." *Environmental Geotechnics*, 1(2), 108-120.

Tiwari, B., and Ajmera, B. (2015). "Reduction in Fully Softened Shear Strength of Natural Clays with NaCl Leaching and Its Effect on Slope Stability." *Journal of Geotechnical and Geoenvironmental Engineering*, 141(1), 1-10.

Yoosefi, S., Jebeli, M., Baker, W. J., and Meehan, C. L. (2024a). "Effect of Initial Osmotic Suction on the Volume Change Behavior of Saturated Soil." *Proc., GeoCongress 2024: Bridging Government, Industry, and Academia for Resilient Mega-Communities*, Vancouver, Canada, February 25-28, 2024, ASCE, Reston, VA. 643-653.

Yoosefi, S., Jebeli, M., Baker, W. J., and Meehan, C. L. (2024b). "Evaluating the Temperature Sensitivity of a Capacitance Sensor for Measuring Soil Volumetric Water Content and Electrical Conductivity." *Proc., Geo-Congress 2024: Bridging Government, Industry, and Academia for Resilient Mega-Communities*, Vancouver, Canada, February 25-28, 2024, ASCE, Reston, VA. 355-365.

Yoosefi, S., Jebeli, M., Baker, W. J., and Meehan, C. L. (2025). "Effect of Pore Fluid Salinity on Isotropic Compressibility, Vertical Permeability, and Triaxial Stress-Strain Behavior of Kaolinite." *Proc., Geotechnical Frontiers 2025: Climate Change*, Louisville, KY, March 2-5, 2025, ASCE, Reston, VA. 1-10.

© ASCE

Assessing Vetiver Grass Impact on Erosion Control and Infiltration of Yazoo Clay under Simulated Extreme Rainfall Conditions

Rahul Biswas[1]; Asef Israk Arnob[2]; Richa Pokhrel[3]; and Sadik Khan, Ph.D., P.E.[4]

[1]Graduate Research Assistant, Dept. of Civil and Environmental Engineering, Jackson State Univ., Jackson, MS (corresponding author). ORCID: https://orcid.org/0009-0002-6977-7881. Email: rahul.biswas@jsums.edu
[2]Graduate Research Assistant, Dept. of Civil and Environmental Engineering, Jackson State Univ., Jackson, MS. Email: J01027856@students.jsums.edu
[3]Graduate Research Assistant, Dept. of Civil and Environmental Engineering, Jackson State Univ., Jackson, MS. Email: richa.rokhrel@students.jsums.edu
[4]Associate Professor, Dept. of Civil and Environmental Engineering, Jackson State Univ., Jackson, MS. Email: sadik.khan@jsums.edu

ABSTRACT

This study presents a large-scale laboratory-based model test on compacted expansive Yazoo clay, commonly found in central Mississippi. Yazoo clay is subjected to high shrink-swell potential with moisture variation due to its unique mineral composition. Under extreme rainfall and heat, Yazoo clay swells upon water infiltration and shrinks during drying, leading to instability in highway slopes across Mississippi. This comprehensive experimental study incorporates real-time sensor monitoring of soil matric potential, moisture content, and bulk electrical conductivity to assess infiltration behavior and the impact of vetiver grass on the slope. A large-scale physical experiment was prepared with a 2:1 slope (Area 2.14 m^2), where vetiver grass was planted during slope construction. Rainfall was simulated for a 100-year return period with an intensity of 1.88 cm/h (12 h duration), according to the National Oceanic and Atmospheric Administration (NOAA). The main objective of this study is to investigate the hydrologic and erosion response of a vegetated Yazoo clay slope with vetiver grass (*Chrysopogon zizanioides*) using sensor trends and LiDAR-based profile evaluation under simulated rainfall. The experimental results showed that 45.54% of the simulated rainfall became surface runoff. Sensor data further indicated high infiltration capacity of the soil, despite Yazoo clay's typically low permeable nature. LiDAR profiles revealed slight slope movement; however, no visible cracks or surface erosion were detected in the immediate post-rainfall scans.

KEYWORDS: Expansive clay, Vetiver grass, Slope stability, Infiltration behavior, LiDAR monitoring, Real-time soil sensors

INTRODUCTION

Global climate change has led to significant impacts in global precipitation patterns which intensifies the frequency and magnitude of extreme rainfall events. Increasing global surface temperatures are very likely to lead to changes in precipitation and atmospheric moisture because of changes in atmospheric circulation, a more active hydrological cycle, and increases in the water-holding capacity throughout the atmosphere. These changes pose serious threats to infrastructure, particularly highway slopes. During the last decade, tremendous efforts in climate modelling have yielded a wide range of climate data (Overpeck et al., 2011). Global climate

© ASCE

models predict a rise in extreme precipitation events due to increased atmospheric moisture content resulting from rising temperatures. This phenomenon leads to higher rainfall intensities over shorter periods, increased variability in seasonal precipitation patterns and greater susceptibility to soil saturation and erosion.

Excessive rainfall with high intensity is mainly responsible for the soil erosion and resultant landslide and slope failure (Sarker & Rashid, 2013). Expansive soils are very sensitive to climate changes due to their significant affinity for water, with the variation of seasonal rainfall pattern serving as the main external cause for shallow slope failures (Xu et al., 2022). Yazoo clay (an expansive clay soil dominant in the central Mississippi region) is calcareous and highly plastic clay soil which is typically with a hard-to stiff consistency at moisture contents near its plastic limit (Nobahar et al., 2019). The average composition of the Yazoo clay is 28% montmorillonite, 24% kaolinite, 22% quartz, 15% calcite, 8% illite, 2% feldspar, and 1% gypsum based on recent X-ray diffraction results (Taylor, 2005). Weathered Yazoo clay has a distinctive yellow-brown color, while unweathered Yazoo clay is blue grey. Shallow slope failure on Yazoo clay is induced due to the climate variation in Mississippi. The amount of total volumetric rainfall attects in the infiltration behavior of highly plastic clay. Typically, a shallow slope failure occurs due to an increase in pore water pressure and a reduction of soil strength due to the progressive wetting of soil near the surface (Nobahar et al., 2019). Successive and extreme high rainfall intensity can have significant influence on inducing the shallow slope failure (Khan et al., 2018).

For controlling erosion and optimizing the slope stability, Vegetation is being popular as nature based solution and a recognized method all over the world (Chikh et al., 2019; Islam et al., 2020). Vetiver grass (*Vetiveria zizanoides*) is one of the plants employed in vegetation-based soil bioengineering for landslide prevention and mitigation. Vetiver grass has long and fibrous roots that can penetrate vertically deep into soil up to 3to 4 m (Hellin and Haigh, 2002). Despite being a tropical plant, Vetiver is adaptable to a variety of climatic and soil conditions, and it can thrive in a variety of temperatures and climates. Vetiver is not resistant to cold and can’t survive freezing temperatures (Yadav, 2010). Typical ranges of environmental stress that vetiver can withstand are a pH 3.3–9.5 and 15 °C to 55 °C (Danh et al., 2009). It was observed that vetiver grass was effective in minimizing the soil loss and maximizing resistance against runoff compared to similar types of grasses (Islam et al., 2021). Donjadee and Tingsanchali, 2013compared surface soil runoff with five different rainfall intensities and they also proposed an empirical equation correlating vertical interval of hedgerows, slope gradient in percent, and runoff volume in millimeter. Ghosh and Bhattacharya, 2018 evaluate the overall performance of vetiver grass for stabilizing the coastal embankment of Bangladesh. Vetiver grass extensive root network enhances soil shear strength, reducing susceptibility to slope failure. Islam and Badhon, 2020 conducted direct shear tests on laboratory reconstituted soil samples to evaluate the shear strength of vetiver-rooted soil. The infiltration capacity of soil under the vegetated vetiver grass is the major parameter that was observed in this study, focusing on the extreme rainfall conditions on fully grown vetiver grass. Previously, there were large-scale lab-based physical modelling experiments conducted with vetiver grass with artificially simulated rainfall but not for extreme rainfall conditions. Soil properties like bulk density, particle density, porosity, field capacity, and hydraulic conductivity influence how much water can seep into the soil (Hossain et al., 2019).

This study investigates the vetiver grass performance on expansive clay in terms of changes in moisture content, matric suction, electric conductivity, SWRC (Soil Water Retention Curve) curve and runoff parameters for rainfall intensity equivalent to the 100-year return period. According to the National Oceanic and Atmospheric Administration (NOAA), the rainfall

© ASCE

intensity for a 100-year return period is 1.88 cm/hr. for the Jackson, Mississippi region. This study evaluated the performance of fully grown vetiver grass and showed that infiltration is increased significantly with the decrease in surface runoff which helps to keep the soil moisture balance in such a condition that eventually keeps the slope stable. Rainfall-induced slope failures are reported to occur either during or immediately following periods of intense or prolonged heavy rainfall (Tohari et al., 2007). With global precipitation patterns becoming more unpredictable due to climate change, it is crucial to prepare for extreme weather conditions.

This study plays a significant role in evaluating the effectiveness of vetiver grass in extreme rainfall scenarios and its potential for erosion control and slope stability. The findings of this study will enrich the development of adaptive strategies for enhancing the long-term resilience of highway slopes against climate-induced challenges.

METHODOLOGY

Test Procedure

A laboratory-scale lysimeter was constructed using a waterproof wooden frame to simulate highway slope conditions and assess infiltration, runoff, and drainage characteristics. The dimension of the lysimeter (Figure 1) was 182.9 cm in length and 50.8 cm in height, with a slope ratio of 1H:1V. The frame's crest and foundation were extended 50.8 cm horizontally, and the foundation was extended vertically by 50.8 cm to minimize potential boundary effects and ensure uniform water flow and infiltration. Wooden members were installed above the frame to provide support for a rainfall simulation system. To facilitate access for dozers and compactors, mental hinges were incorporated into the design, allowing the front panel to function as a drop-down door.

To retain moisture and control infiltration within the system, a 0.5 mm-thick geomembrane was installed along the base and side walls of the lysimeter. The drainage base, consisting of a 15.2 cm layer of pea gravel, was designed at the bottom of the lysimeter. Perforated pipes, 10.2 cm in diameter, were embedded within this drainage base to facilitate water collection and discharge. A nonwoven geotextile layer was placed over the drainage base to act as a separator between the drainage layer and the overlying clay soil. To capture and measure both runoff and infiltrated water, a network of polyvinyl chloride (PVC) tubes and polyethylene (PEX) tubing was used. Perforated pipes in the drainage base were fitted with 1.3 cm diameter PVC outlets, which connected to collection buckets with a capacity of 5 gallons. The connections were made using 0.64 cm PEX tubing to ensure precise flow routing to the collection containers. The lysimeter was filled with compacted clay layers to replicate natural soil conditions. Meter group 'Teros12' and 'Teros 21' Sensors were used in this study to continuously monitor several soil properties, including soil matric potential, moisture content, and electric conductivity. The fully-grown Vetiver Grass root extended up to 38.1 cm in some areas. To get the data from the differential level, the sensors were installed at 15.2 cm and 45.7 cm depths (Figure 1). These sensors were selected due to their high accuracy, durability, and ability to provide real-time in-situ measurements. The Teros 12 sensor uses capacitance/frequency-domain reflectometry (FDR) to monitor temperature, electrical conductivity (EC), and volumetric water content (VWC). It offers high-precision soil moisture data, essential for comprehending water retention and infiltration characteristics. Similarly, Teros 21 is a tensiometer-based sensor used to measure matric potential of soil. It is particularly effective in unsaturated soils, providing real-time data on soil water availability. Data was recorded every 15 minutes using a Zentra logger 6 (ZL6).

© ASCE

Five rows of vetiver grass slips were planted along the slope face of the lysimeter (Figure 1), with a total of 55 slips. Each slip was planted using a peat moss mixture to promote root establishment. To prevent erosion and the displacement of topsoil and nutrients, small quantities of water were carefully sprinkled onto the slope using small containers instead of water hoses. For the rainfall simulation, 1.88 cm PEX tubing clamped onto the overhead wooden frame. The tubing was fitted with 0.8 mm diameter nozzles, which were arranged in three rows containing a total of 28 nozzles to ensure uniform distribution of precipitation across the lysimeter surface. The water supply for the rainfall simulation was provided by a 300-gallon intermediate bulk container placed on a steel frame 1.83 m above the ground with a flow regulatory meter to provide uniformity of rainfall distribution (Figure 1).

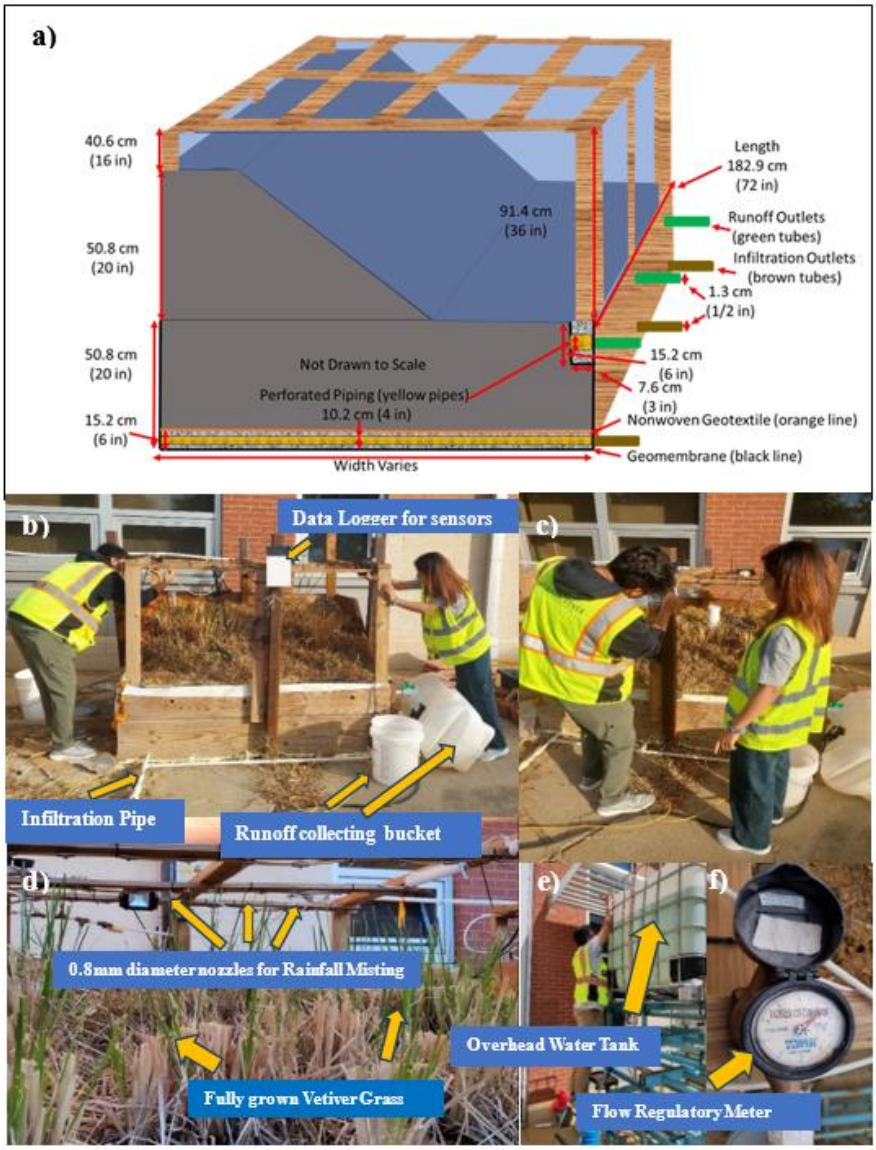


Figure 1: a) Schematic Diagram of Test Frame, (b) Rainfall Lysimeter with Wooden Frame (Front View), c) Sensor Data Collection, d) Misting Nozzle Setup for Simulating Rainfall, e) Overhead Tank, f) Discharge Measuring Meter.

© ASCE

Terrestrial LiDAR was utilized both before and after the test to capture high-resolution topographic changes, allowing precise assessment with point cloud data of soil surface to investigate the surface modifications and erosion patterns influenced by the extreme rainfall.

Precipitation Pattern

To determine the appropriate rainfall intensity for Jackson, Mississippi, NOAA's Precipitation Intensity-duration-Frequency (IDF) curves were utilized. In this study, the selection of 1.88cm/hr. rainfall intensity is based on the 100-year return period, which corresponds to extreme precipitation events once in a century. The curves indicate that precipitation intensity increases with a more extended return period. The 100-year return period intersects with various storm durations, aligning with our chosen value of 1.88cm/hr. These curves represent precipitation intensity across different storm durations. For this study, the 100-year return period shows that for a relevant storm duration, the precipitation intensity aligns with 1.88cm/hr.

RESULTS AND DISCUSSION

This study's findings are presented using sensor-based measurements to assess the infiltration capacity of vegetated soil and LiDAR-based profile assessments to evaluate slope behavior under extreme rainfall simulation. The integrated approach provides insights into the role of vegetation in slope stability, moisture retention, and infiltration dynamics.

LiDAR Profile Comparison

With LiDAR profiles, slope movement and stability can be precisely and effectively monitored using real-time point cloud data. These profiles offer a thorough topographic evaluation of the slope before and after any extreme event. This study has compared the LiDAR profile of the test frame slope to observe any considerable surface erosion or visible cracks on the slope profile during and after the rainfall simulation.

As shown in Figure 2, three cross-sectional slope profiles were extracted at consistent intervals- Centerline, left (1 ft offset), and right (1 ft offset). Each subplot presents elevation versus horizontal distance for "Before" and "After" the rainfall simulation. While no major surface erosion or cracking was detected, the LiDAR profiles reveal slight elevation shifts in each section of the slope surface, suggesting minor topographic variations. These subtle changes, while not severe, offer early indications of surface responsiveness under extreme rainfall loading. However, these profiles confirm that the slope is mostly intact and stable even after going through severe rainfall events, strengthening the claim that vetiver grass as vegetation can be effective in stabilizing slopes.

Soil Moisture Variation

The study observes a gradual rise in the moisture content during the rainfall period.

Figure 3 represents a minimal runoff and more infiltration due to a steady increase in the moisture content. The steady post-rainfall moisture content indicates water retention in the soil. Additionally, the steady trend without sudden drops or spikes indicated that the slope is stable and not losing soil particles or water through rapid erosion.

© ASCE

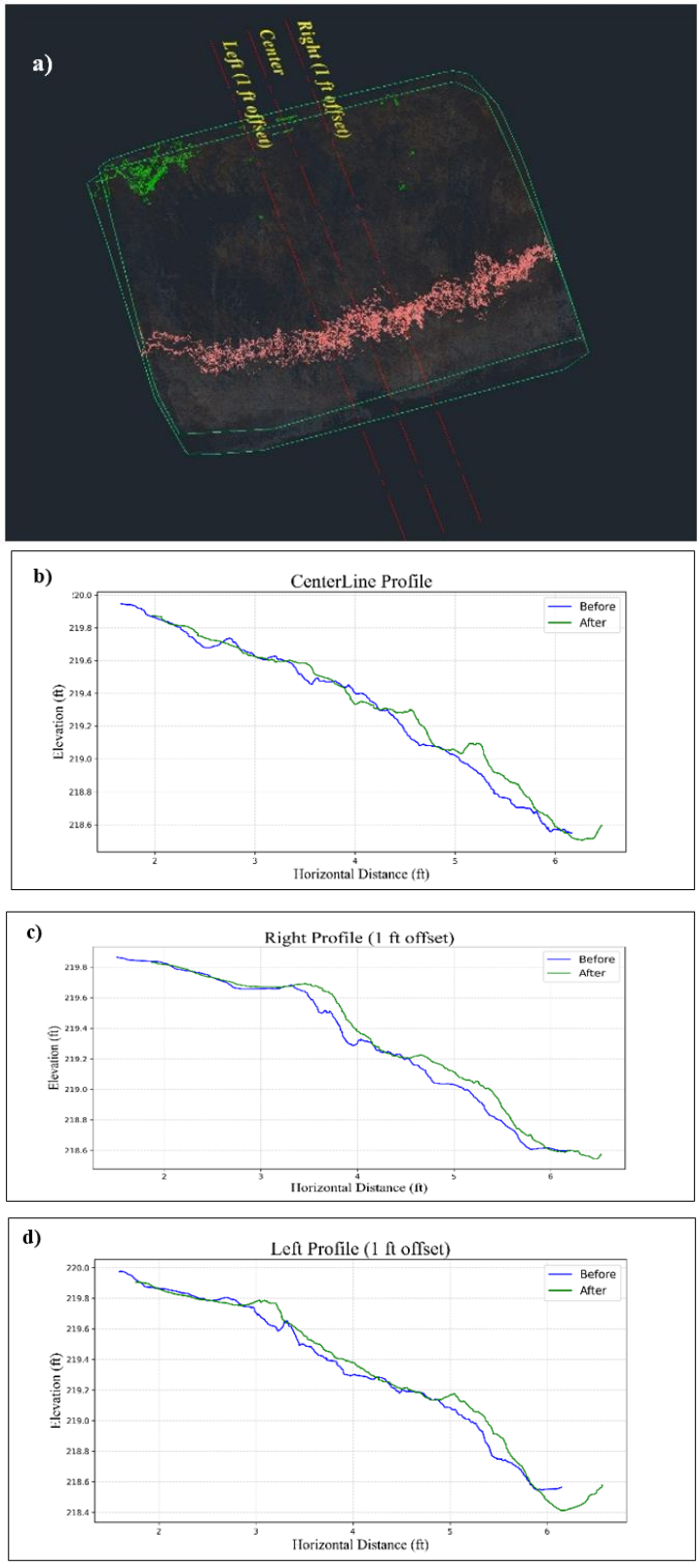


Figure 2: Comparative LiDAR Profiles (a)Superimposed, b) Center Line, c) Right, d) Left Profile (Before and After the Rainfall Simulation)

© ASCE

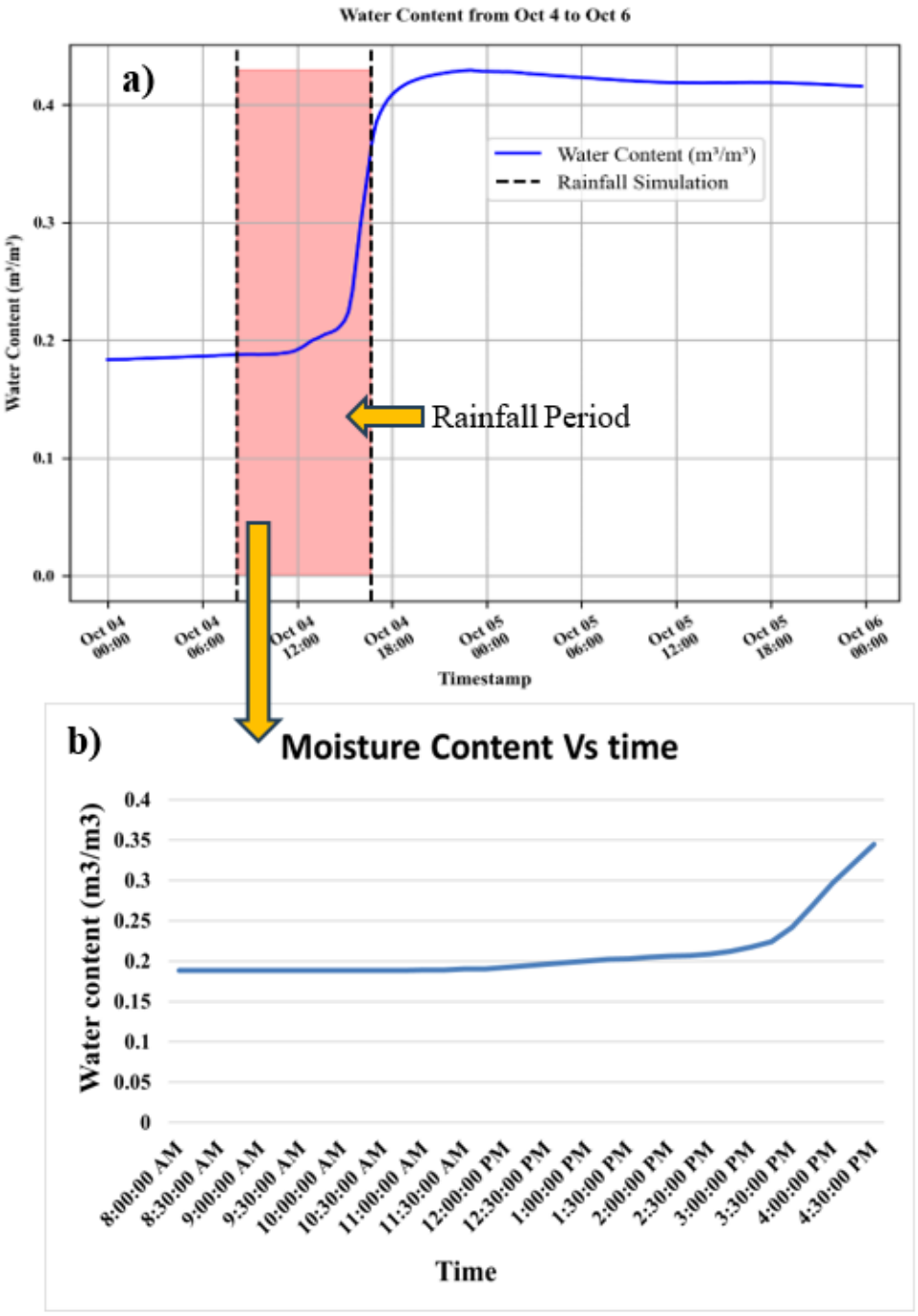


Figure 3: a) Moisture Content Variation from Oct 4 to Oct 6, b) Moisture Content Variation for the Test Period

Variation in Matric Potential

This study observed a sudden fall in soil matric potential during testing (Figure 4). The steep rise in matric potential during testing indicates water infiltration into the soil, reducing soil suction and highlighting water retention capacity. A significant shift occurs in the early afternoon

© ASCE

as matric potential rapidly increases toward 0 kPa, suggesting near-saturation conditions as water content increases (Figure 6b). The steep rise of the curve indicates that the soil retains moisture effectively before reaching near saturation, which can be achieved by the dense root system of the vetiver grass. Vetiver grass dense root system enhances soil permeability, allows deeper water infiltration, reinforces the soil structure, and prevents erosion. Without vetiver grass, the soil likely retained higher suction (more negative matric potential), leading to increased surface runoff due to reduced infiltration. The delayed and sustained moisture retention in the latter half of the test indicated the vetiver's role in slowing down water loss and long-term soil moisture stability, which provides resilience against extreme rainfall events.

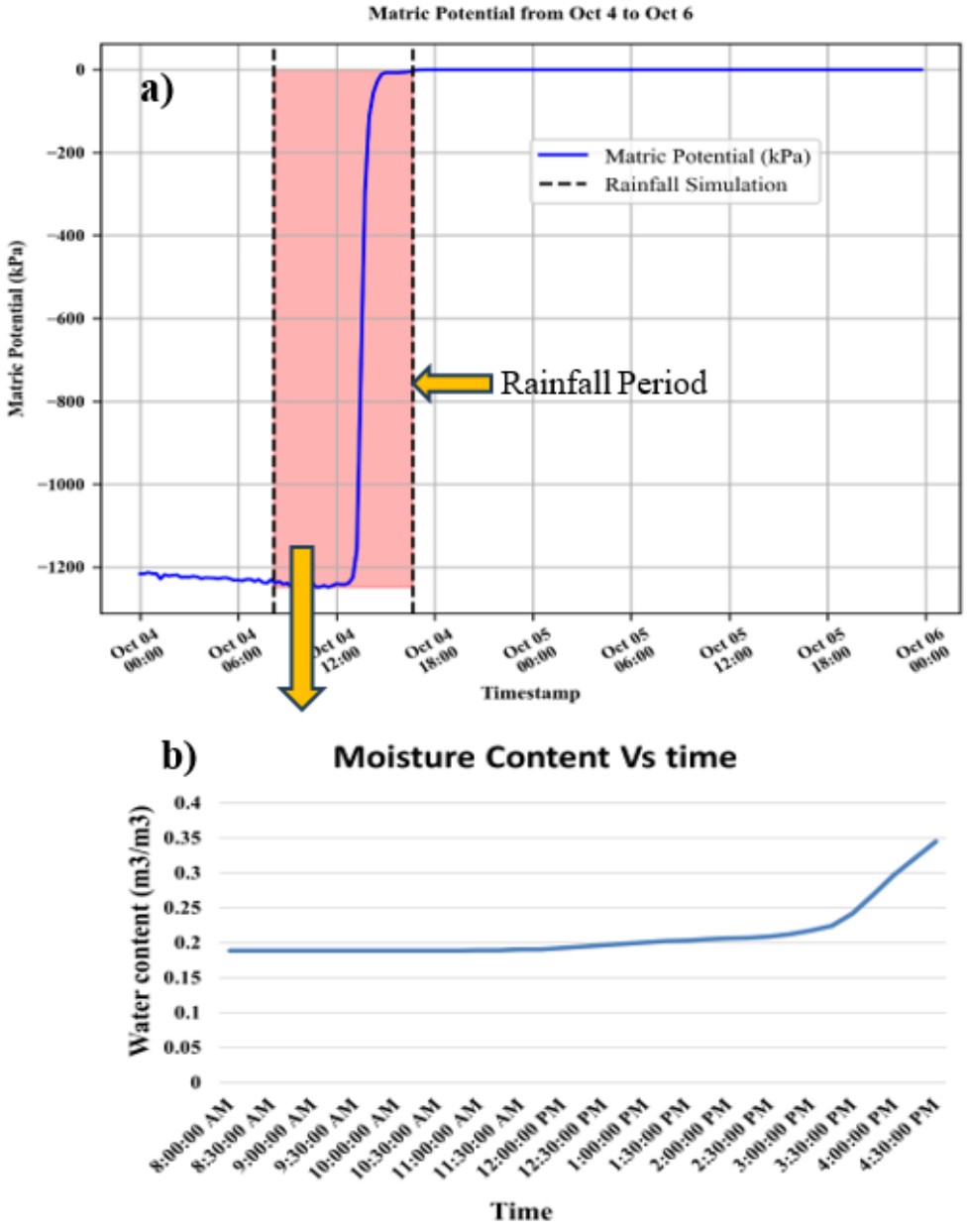


Figure 4: a) Soil Matric Potential Variation from Oct 4 to Oct 6, b) Moisture Content Variation for the Test period

© ASCE

Variation in Electric Conductivity

This study observed an increasing trend in the conductivity value. The increase in conductivity during testing hours reflects enhanced ion mobility caused by water infiltration, validating the soil's infiltration efficiency under vegetated conditions. The gradual rise in Bulk EC after testing hours suggests increased pore water content enhances ion mobility, contributing to higher conductivity values. This trend is not necessarily due to the introduction of new dissolved ions, but rather improved ionic transport due to increased water content in the soil. These findings demonstrate the soil's sustained infiltration and water retention capacity

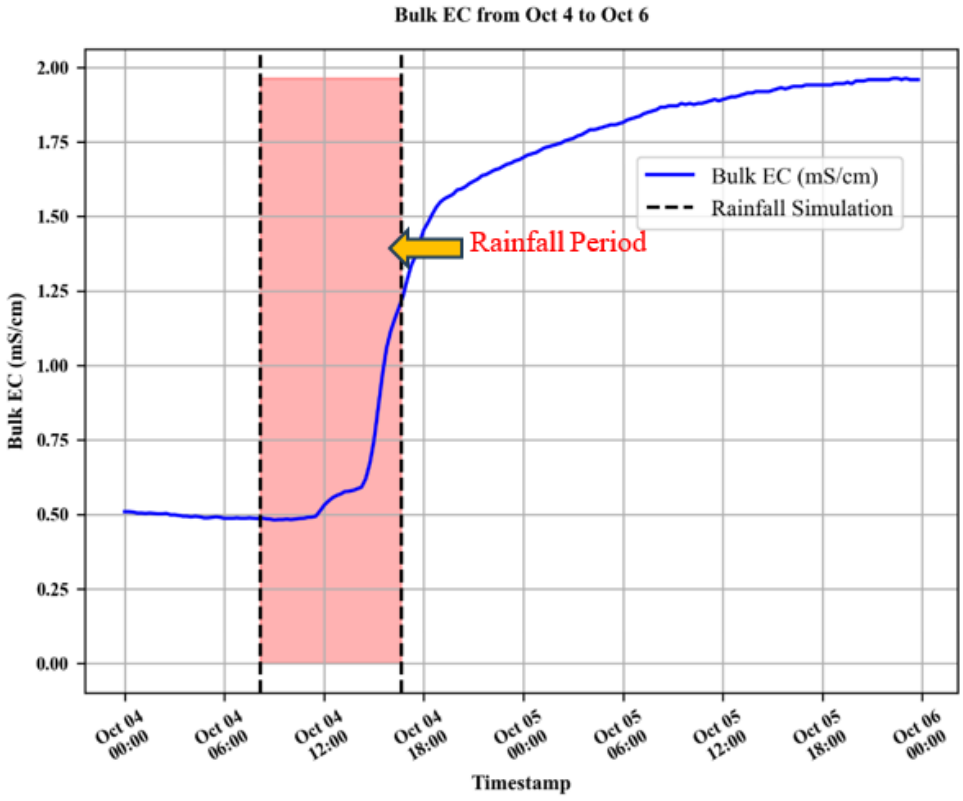


Figure 5: Variation of Electric Conductivity vs Time

Soil Water Retention Curve (SWRC)

The Soil Water Retention Curve (SWRC) describes the relationship between soil matric potential (kPa) and volumetric water content (m^3/ m^3). This curve is essential for understanding the soil's ability to retain and release water under different moisture conditions. The curve exhibits a distinct S-shape, highlighting different moisture retention zones. At high water content levels between approximately 0.25 and 0.35 m^3/ m^3, the soil remains nearly saturated, and matric potential values are close to zero, meaning minimal suction is needed to extract water. A critical transition occurs at around 0.22 and 0.20 m^3/ m^3, where a sharp drop in water content is observed, with matric potential decreasing drastically from approximately -100 to -1400 kPa. The presence of vetiver grass significantly influences the soil water retention curve by improving soil structure and increasing water holding capacity, particularly in the mid-range moisture

© ASCE

content region. The matric potential remains less negative at moderate moisture levels, suggesting that soil with vetiver retains more water for a longer duration compared to bare soil.

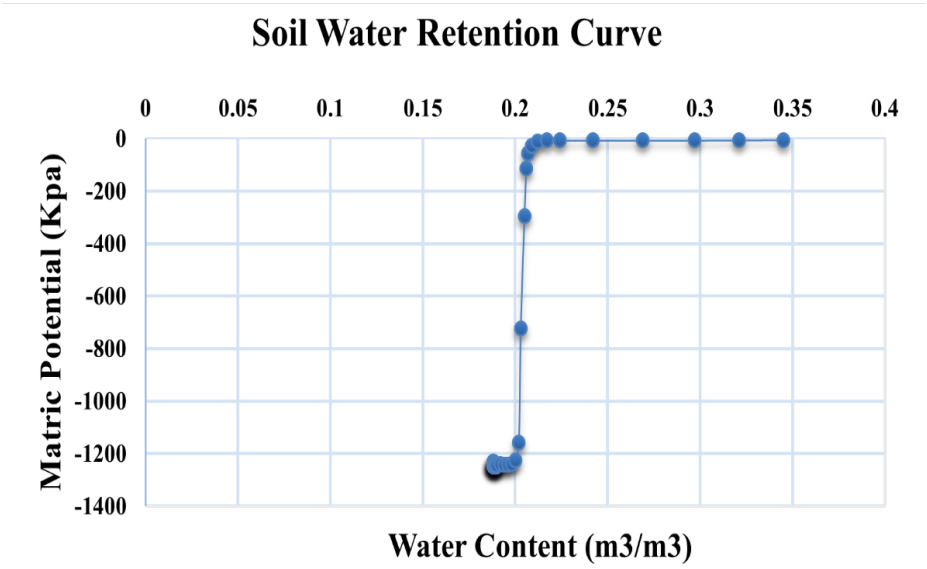


Figure 6: Soil Water Retention Curve During the Test Period

CONCLUSIONS

This study investigates the role of vetiver grass in influencing soil infiltration, matric suction, and overall slope stability in expansive Yazoo clay. This investigation has simulated rainfall for a 100-year return period. During the rainfall simulation period, a gradual increase in the soil moisture content was observed. Consistent moisture retention after the rainfall was also observed. A sharp drop in matric suction was observed when moisture content reached a critical limit (0.2 ~ 0.25 m^3/m^3), indicating rapid saturation beyond that point. Despite the sudden drop in matric suction, no slope instability was detected from comparing the LiDAR point clouds before and after the test period. This study has also observed an increasing trend in the electric conductivity value, indicating enhanced ion mobility. A gradual increase in the conductivity value was also observed even after the rainfall simulation. In this study, the simulated rainfall volume was approximately 127.32 gallons, and the total surface runoff we collected was approximately 57.99 gallons (45.54%). Cross-sectional profiles obtained from LiDAR scans revealed only minor elevation shifts across the slope, with no visible cracking or erosion, confirming slope stability under extreme rainfall. The study's overall findings highlight vetiver grass's potential as an environmentally beneficial way to stabilize slopes in expansive clay soils. The sharp drop in matric suction and sustained moisture retention observed during rainfall simulation are characteristic responses of expansive soils under wetting conditions (Ya, Hongri, Guiyao, & Yanqi, 2024). Additionally, the real-time monitoring capabilities of the TEROS 12 and 21 sensors effectively captured dynamic changes in moisture content, matric suction, and electrical conductivity. These sensor-based observations provided critical insight into infiltration behavior and slope response, reinforcing their applicability for future slope stability monitoring systems.

© ASCE

LIMITATIONS AND FUTURE SCOPE

This study focused solely on the hydrologic and erosion response of a vegetated slope. While findings highlight the potential role of vetiver grass in infiltration and erosion mitigation, no parallel testing was conducted on bare soil at this phase. However, the authors fully intend to conduct an investigation on a vegetated and a bare slope (control section) to compare the results. Additionally, Given Yazoo clay's expansive nature, future studies should investigate the performance of vetiver grass under alternating wetting and drying conditions to better understand its effectiveness in real-world expansive soil environments.

ACKNOWLEDGMENTS

The authors sincerely acknowledge the National Science Foundation (NSF) CMMI (Award No. 2046054) for supporting the study of climate resiliency of highway slopes and Vetiver in landslide repair.

REFERENCES

Chikh, H. A., Habi, M., and Morsli, B. (2019). Influence of vegetation cover on the assessment of erosion and erosive potential in the Isser marly watershed in northwestern Algeria—Comparative study of RUSLE and PAP/RAC methods. *Arabian Journal of Geosciences*, 12(5), 154.

Danh, L. T., Truong, P., Mammucari, R., Tran, T., and Foster, N. (2009). Vetiver Grass, *Vetiveria Zizanioides*: A Choice Plant for Phytoremediation of Heavy Metals and Organic Wastes. *International Journal of Phytoremediation*, 11(8), 664–691.

Donjadee, S., and Tingsanchali, T. (2013). Reduction of runoff and soil loss over steep slopes by using vetiver hedgerow systems. *Paddy and Water Environment*, 11(1–4), 573–581.

Dore, M. H. I. (2005). Climate change and changes in global precipitation patterns: What do we know? *Environment International*, 31(8), 1167–1181.

Ghosh, C., and Bhattacharya, S. (2018). Landslides and Erosion Control Measures by Vetiver System. In I. Pal & R. Shaw (Eds.), *Disaster Risk Governance in India and Cross Cutting Issues* (pp. 387–413). Springer Singapore.

Hellin, J., and Haigh, M. J. (2002). Better land husbandry in Honduras: Towards the new paradigm in conserving soil, water and productivity. *Land Degradation & Development*, 13(3), 233–250.

Hossain, A., Chowdhury, M. E., and Islam, M. (2019). Evaluation of the effect of rainfall on slope stability analysis by using hydraulic unit flux infiltration property.

Islam, M. A., Islam, M. S., Chowdhury, M. E., and Badhon, F. F. (2021). Influence of vetiver grass (Chrysopogon zizanioides) on infiltration and erosion control of hill slopes under simulated extreme rainfall condition in Bangladesh. *Arabian Journal of Geosciences*, 14(2), 119.

Islam, M. S., and Badhon, F. F. (2020). A Mathematical Model for Shear Strength Prediction of Vetiver Rooted Soil. *Geo-Congress 2020*, 96–105.

Islam, M. A., Islam, M. S., and Elahi, T. E. (2020). Effectiveness of Vetiver Grass on Stabilizing Hill Slopes: A Numerical Approach. *Geo-Congress 2020*, 106–115.

© ASCE

Khan, M. S., Nobahar, M., Ivoke, J., and Amini, F. (2018). Rainfall Induced Shallow Slope Failure over Yazoo Clay in Mississippi. *PanAm Unsaturated Soils 2017*, 153–162.

Nobahar, M., Khan, M. S., Ivoke, J., and Amini, F. (2019). Impact of Rainfall Variation on Slope Made of Expansive Yazoo Clay Soil in Mississippi. *Transportation Infrastructure Geotechnology*, 6(4), 318–336.

Overpeck, J. T., Meehl, G. A., Bony, S., and Easterling, D. R. (2011). Climate Data Challenges in the 21st Century. *Science*, 331(6018), 700–702.

Sarker, A. A., and Rashid, A. K. M. M. (2013). Landslide and Flashflood in Bangladesh. In R. Shaw, F. Mallick, & A. Islam (Eds.), *Disaster Risk Reduction Approaches in Bangladesh* (pp. 165–189). Springer Japan.

Taylor, A. C. (2005). *Mineralogy and engineering properties of the Yazoo Clay Formation, Jackson Group, Central Mississippi* [M.S., Mississippi State University]. In ProQuest Dissertations and Theses (305418040). ProQuest Dissertations & Theses Global. https://www.proquest.com/dissertations-theses/mineralogy-engineering-properties-yazoo-clay/docview/305418040/se-2?accountid=11661.

Tohari, A., Nishigaki, M., and Komatsu, M. (2007). Laboratory Rainfall-Induced Slope Failure with Moisture Content Measurement. *Journal of Geotechnical and Geoenvironmental Engineering*, 133(5), 575–587.

Xu, Y., Su, C., Huang, Z., Yang, C., and Yang, Y. (2022). Research on the protection of expansive soil slopes under heavy rainfall by anchor-reinforced vegetation systems. *Geotextiles and Geomembranes*, 50(6), 1147–1158.

Yadav, S. K. (2010). Cold stress tolerance mechanisms in plants. A review. *Agronomy for Sustainable Development*, 30(3), 515–527.

Ya, Z., Hongri, Z., Guiyao, W., and Yanqi, Y. (2024). The infiltration characteristics of expansive soil considering fracture under wet-dry cycle conditions. *Heliyon*, 10(17).

© ASCE